Objective pilling evaluation of nonwoven fabrics

Junmin Zhang, Xungai Wang

Centre for Material and Fibre Innovation, Deakin University, Geelong, Victoria, 3217, Australia

Stuart Palmer

Institute of Teaching and Learning, Deakin University, Waterfront campus, Geelong, Victoria, 3220, Australia

Abstract

A pilled nonwoven fabric image consists of brightness variations caused by high frequency noise, randomly distributed fibers, fuzz and pills, fabric surface unevenness, and background illumination variance. They have different frequency and space distributions and thus can be separated by the two-dimensional dual-tree complex wavelet transform reconstructed detail and approximation images. The energies of the six direction detail sub-images, which capture brightness variation caused by fuzz and pills of different sizes, quantitatively characterize the pilling volume distribution at different directions and scales. They are used as pilling features and inputs of neural network supervised classifier. The initial results based on a nonwoven wool fabric standard pilling test image set, the Woolmark® SM 50 Blanket set, suggest that this objective pilling evaluation method developed by the combination of pilling identification, characterization method and neural network supervised classifier is feasible.

KEY WORD: nonwoven, pilling, objective evaluation, complex wavelet transform, neural network

INTRODUCTION

The development of practical and commercial nonwoven wool fabrics is a significant innovation, creating “fabrics with unique properties that cannot be achieved by traditional knitting or weaving, opens up a whole new range of market opportunities for Merino wool” [1]. However the success of

nonwoven wool fabrics or apparels would particularly depend on the overcoming of the pilling problem. A key element in the control of fabric pilling is the evaluation of resistance to pilling by testing. Normally the resistance to pilling of nonwoven fabrics is tested in the Martindale Abrasion Tester (see ISO:12947-1 Martindale abrasion testing apparatus). The sample is abraded for a specified number of rotations that simulate accelerated wear, and the surface change is evaluated by experts based on a visual comparison of the sample to a photographic standard.

Contrary to the regular yarn interlacing pattern in woven and knitted fabrics, nonwoven fabric is a fibrous web of randomly orientated fibers, bonded by friction, and/or cohesion and/or adhesion as defined by ISO 9092. As nonwoven fabrics differ from woven and knitted fabrics in structure, the presence of inter-fiber bonds limits the available fiber length and leads to more fuzz than pills in nonwoven fabrics [2]. The developed pilling rating systems based on woven and knitted fabrics may not suitable for nonwoven fabrics.

Palmer and Wang [3] conducted research on objective evaluation of nonwoven fabric pilling. Based on a nonwoven wool fabric standard pilling test image set, the Woolmark® SM 50 Blanket set, they proposed that the standard deviation of the distribution of the wavelet approximation coefficients at wavelet analysis scale 5 has a monotonic relationship with the pilling intensity. The wavelet coefficients are results from convolving the fabric image columns or rows with the wavelet functions. To reduce the risk that the analyzing wavelet function's structure is misinterpreted as a characteristic of the pilled fabric image, the wavelet should be chosen in accordance with the intrinsic structure presented in the pilled fabric image. It was noticed that the wavelet coefficients of a signal are very sensitive to translations of the signal [4]. A small shift of an image greatly perturbs the wavelet coefficient oscillation pattern around brightness variation points in the image.

In this study, an objective pilling evaluation method based on two-dimensional dual-tree complex wavelet transform (2DDTCWT) [4] and supervised classification is proposed. The pilling in

nonwoven fabrics is identified by the reconstructed detail images excluding those that represent high frequency noise and random fiber structure, and low frequency fabric surface unevenness and background illumination variance, and the energies of the six direction detail sub-images of the identified pilling are used as pilling features to characterize the pilling. The initial verification based on a nonwoven wool fabric standard pilling test image set, the Woolmark® SM 50 Blanket set, suggests that the pills and fuzz can be identified by the reconstructed detail images at different scales, and the pilling features extracted from the detail sub-images yield excellent pilling grades classification.

MATERIALS AND SAMPLE PREPARATION

The WoolMark® standard nonwoven pilling test image set, the SM 50 Blanket set, has four test images for each pilling grade. For each pilling grade (1 to 5), four sample images of 512×512 pixels were obtained (see Figure 1). The circular pilling area is tangent to the outside square of the sample images so that sample images include all the pilling information.

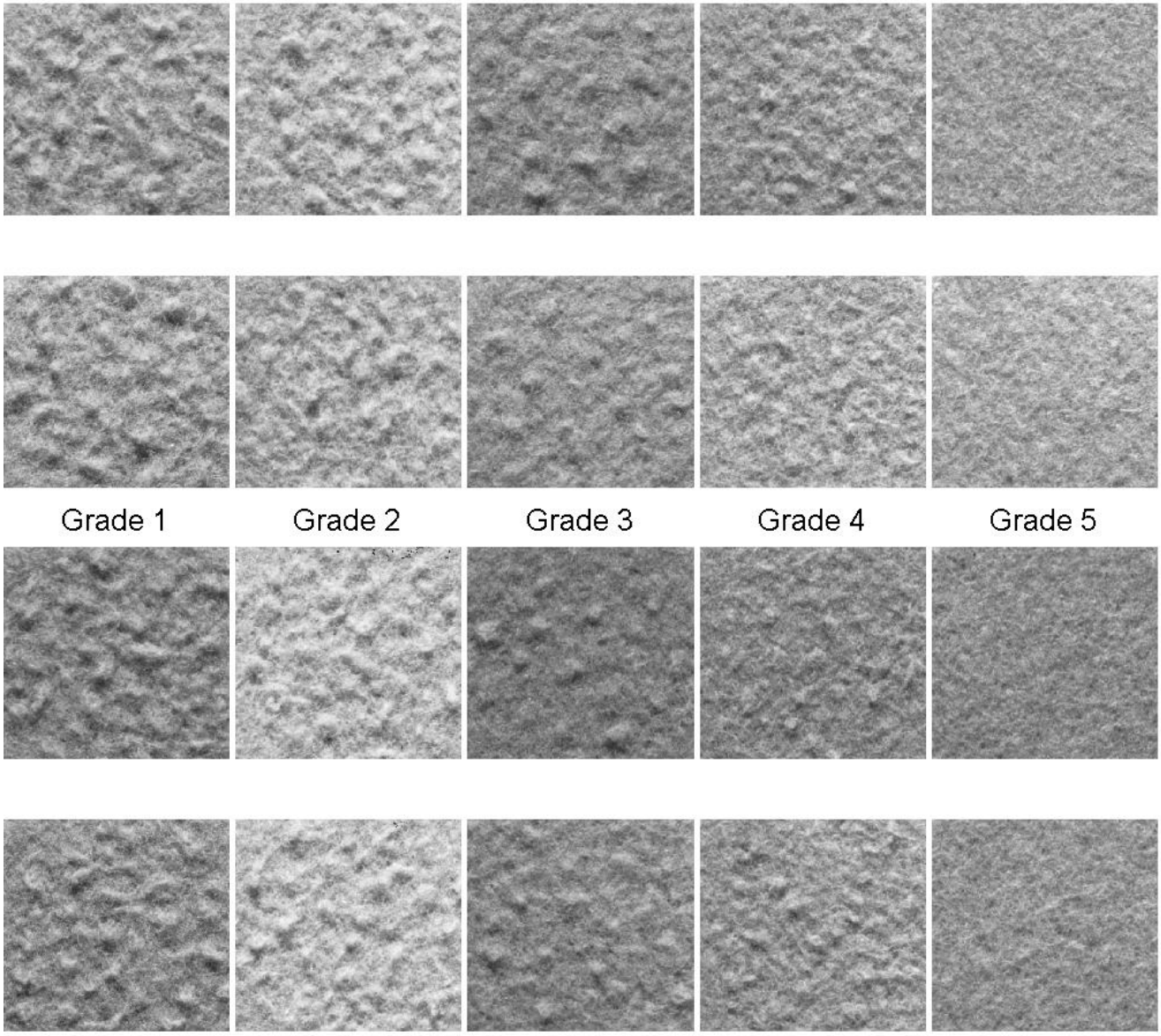

Figure 1. Prepared image samples from the WoolMark® standard nonwoven pilling test image set

NONWOVEN FABRIC PILLING IDENTIFICATION

The two dimensional dual-tree complex wavelet transform (2DDTCWT) [4] is an enhancement to the two dimensional discrete wavelet transform, it yields nearly perfect reconstruction, approximate analytic wavelet basis and directional selectiveness (±15º, ±45º, ±75º) in two dimensions. Figure 2 represents the reconstructed detail and approximation images of pilling grade 1 nonwoven standard pilling test image by the 2DDTCWT. The 2DDTCWT is performed using the wavelet software from Brooklyn Polytechnic University, NY [5] and Matlab® Wavelet Toolbox [6, 7]. From left to

right and the top down, they are scale 1 to 7 detail images, scale 7 approximation image and the original sample image. From these reconstructed detail and approximation images, it is observed that the scale 7 detail and approximation images detect the fabric surface unevenness and the background illumination variance respectively, the first three scale detail images represent the high frequency noise and random fiber distribution, while scale 4 to 6 detail images capture the pilling (fuzz and pills) of different sizes.

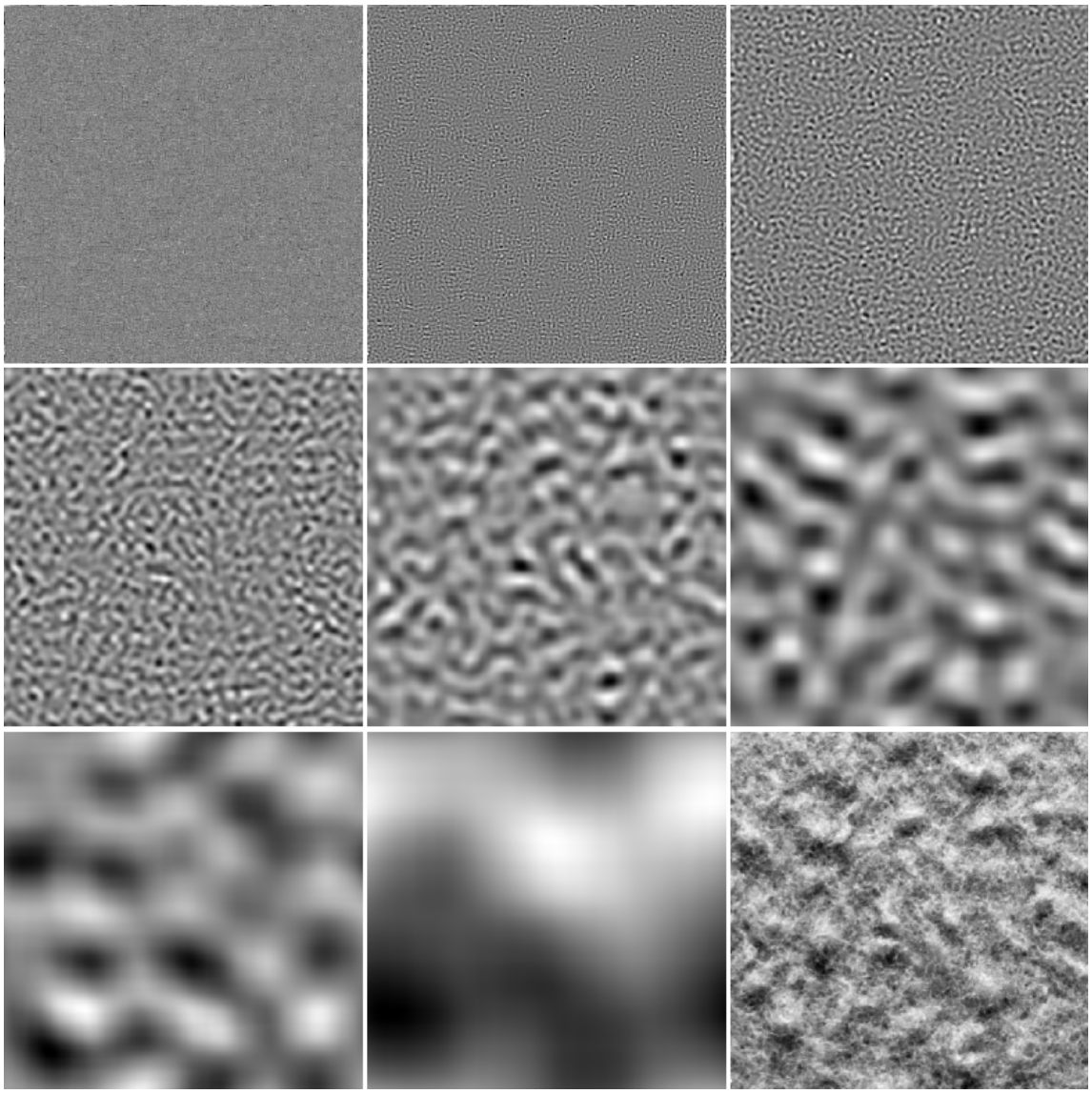

Figure 2. Reconstructed scale 1 to 7 detail images and scale 7 approximation image of pilling grade 1 nonwoven sample image by 2DDTCWT

PILLING CHARACTERIZATION

Whereas the scale and gray intensity value of the detail images represent the size and height of pilling, the shape of pilling can be more efficiently represented by the six direction detail sub-images. The energies of the six directional (±15º, ±45º, ±75º) detail sub-image at scale 4 to 6 are thus used as pilling features. The energy of a reconstructed detail sub-image is defined as:

$$E_{jk} = \frac{1}{M \times N} \sum_{m,n}^{M,N} \left(D_j^k (m,n) \right)^2 \left(4 \le j \le 6, k = \pm 15°, \pm 45°, \pm 75° \right) \qquad (1)$$

Where MxN is the size of the detail sub-image, $D_j^k(m,n)$ are the pixel gray values of detail sub-image in scale j and direction k.

With principal component analysis (PCA), the representative pilling features can be extracted from the 18 pilling features. Figure 3 shows that the first principal component accounts for 81.56% of the total variance of the 18 pilling features, the second principal component explains 7.16 % and the third one 3.59%. Together the first three principal components account for 81.56% + 7.16% + 3.59% or 92.31% of the variance in the 18 pilling features. The scree plot (eigenvalue versus eigenvalue number see Figure 3) shows that a steep slope is evident from the first to the second, and from the second to the third principal component, while the fourth through to the 18th points can be fitted well by a straight line of negligible slope. So the first three principal components that account for 92.31% of the variation are selected to represent all 18 pilling features.

Table 1 presents the correlation coefficients of the 18 pilling features with the first three principal components. The bold font figures indicate the pilling features that significantly correlate with the principal component, and they are the representative pilling features that discriminate among the pilling grades. The score plots of the first principal component versus the second one and the third one are shown in Figure 4. The first principal component has negative correlation with scale 5 and 6

pilling features. The reason for the negative correlation is that grade 1 represents the most severe pilling and thus the grade 1 fabric image has the largest pilling volume or energy. The first principal component produces a progressive separation line between samples of grade 1 and 2, grade 3 and 4, and grade 5 (see Figure 4). It can be expected from Figures 5 that when the pilling grade decreases or the pilling is more severe, scale 5 and 6 detail images capture more pilling of larger size and higher density. The second principal component that has positive correlation with scale 4 and 5 pilling features and negative correlation with scale 6 pilling features discriminates between samples of pilling grade 3 and 4. This is because the grade 4 fabric has slightly small surface fuzzing and partially formed small pills, and they are distributed at scales 4 and 5 (see Figure 5), while the grade 3 fabric has moderate surface fuzzing and pills that are mainly captured in scale 6 detail image (see Figure 5). The third principal component separates grade 1 samples from grade 2 samples. The grade 1 samples' distribution at the negative axis also indicates that the pilling features detect the increasing trend of the pilling intensity and pilling volume with increasing energy.

From the above analysis, it is concluded that the pilling feature vector quantitatively characterizes the pilling volume distribution in six directions and three scales.

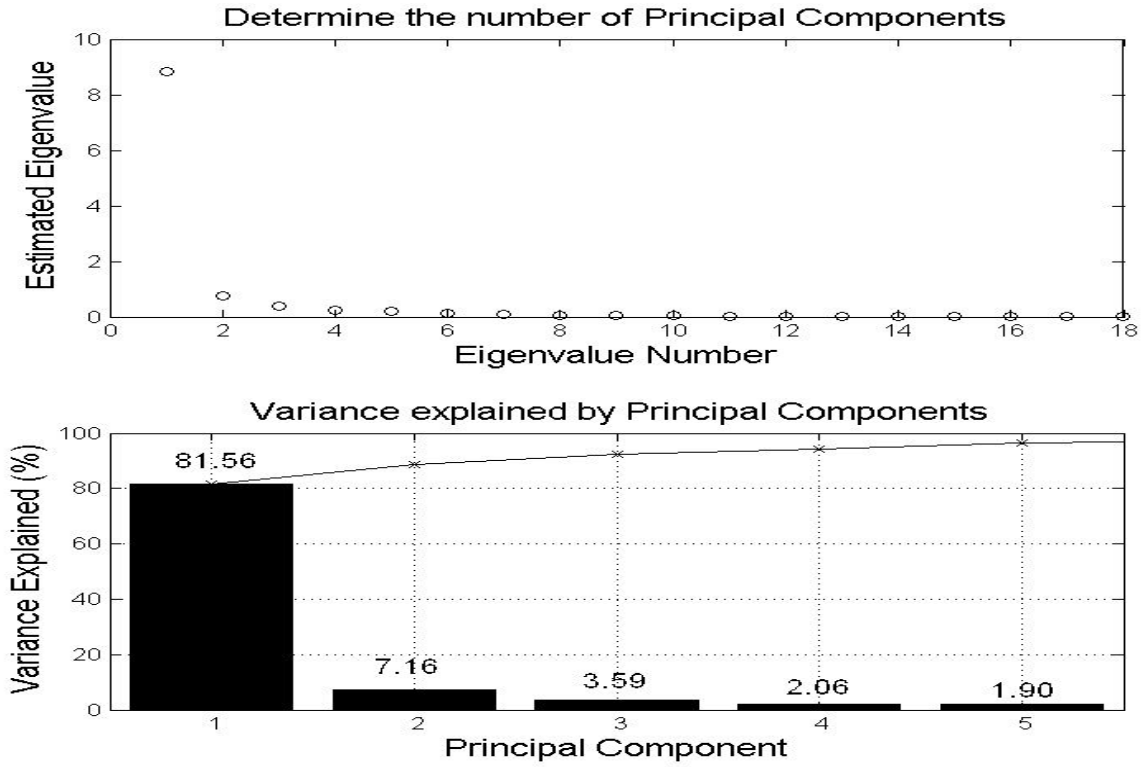

Figure 3. Determination of the number of principal components

Principal Component		**1st**	**2nd**	**3rd**
Scale 4	**−75º**	-0.07	**0.23**	0.04
	−45º	-0.03	0.17	-0.06
	−15º	-0.05	**0.34**	-0.05
	+15º	-0.06	**0.31**	0.06
	+45º	-0.01	0.13	0.06
	+75º	-0.06	0.08	0.17
Scale 5	**−75º**	**-0.2**	0.16	0.07
	−45º	-0.1	**0.3**	-0.06
	−15º	**-0.31**	**0.44**	-0.16
	+15º	**-0.28**	0.13	-0.06
	+45º	-0.12	0.13	0.08
	+75º	-0.17	0.13	**0.28**
Scale 6	**−75º**	-0.18	-0.12	-0.11
	−45º	**-0.3**	**0.2**	**-0.27**
	−15º	**-0.46**	**-0.37**	**-0.58**
	+15º	**-0.49**	**-0.29**	**0.51**
	+45º	**-0.28**	-0.02	**0.4**
	+75º	**-0.25**	**-0.23**	-0.01

Table 1. Correlation coefficients of the pilling features with the first three principal components

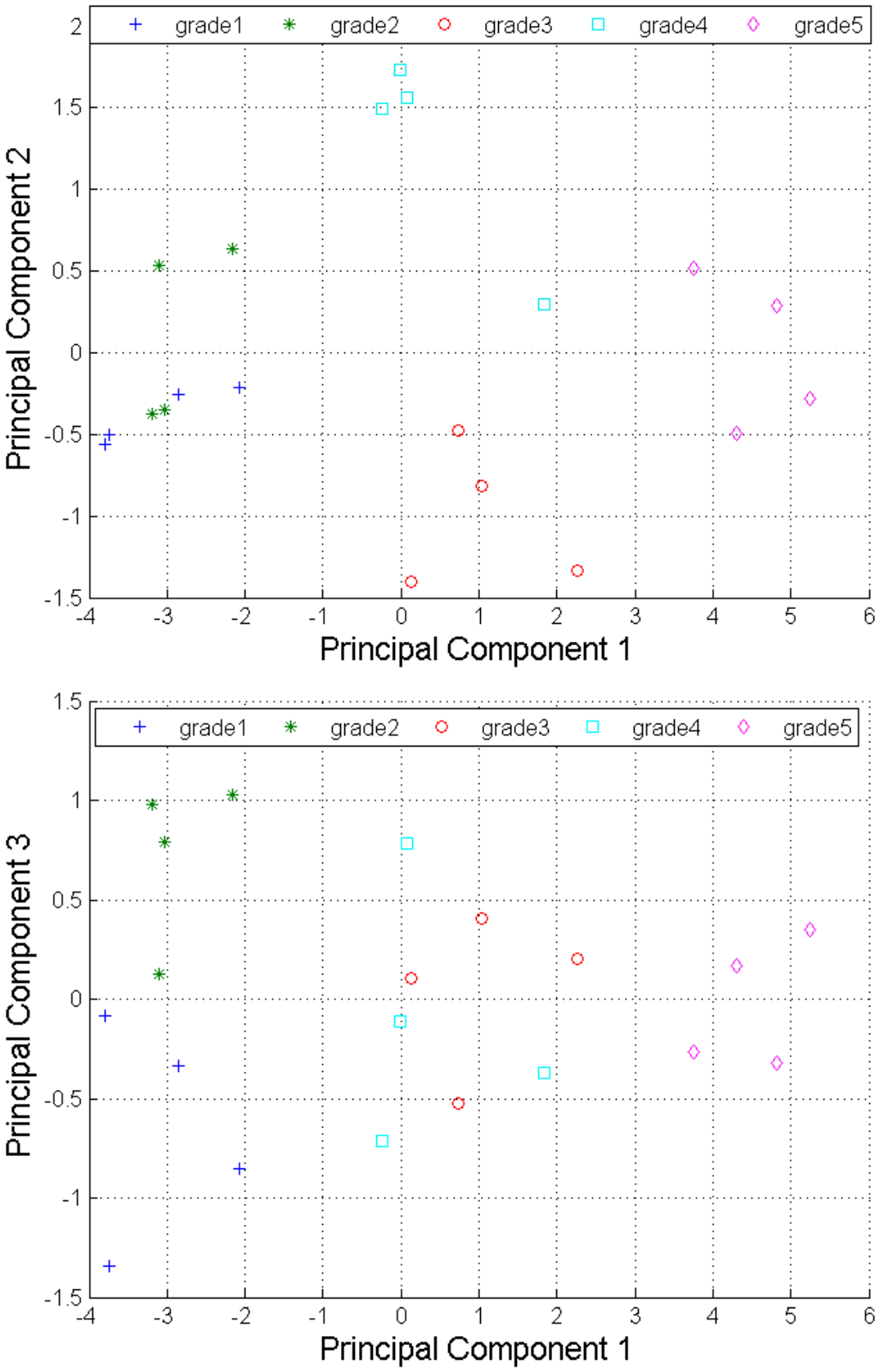

Figure 4. Plots of principal component scores

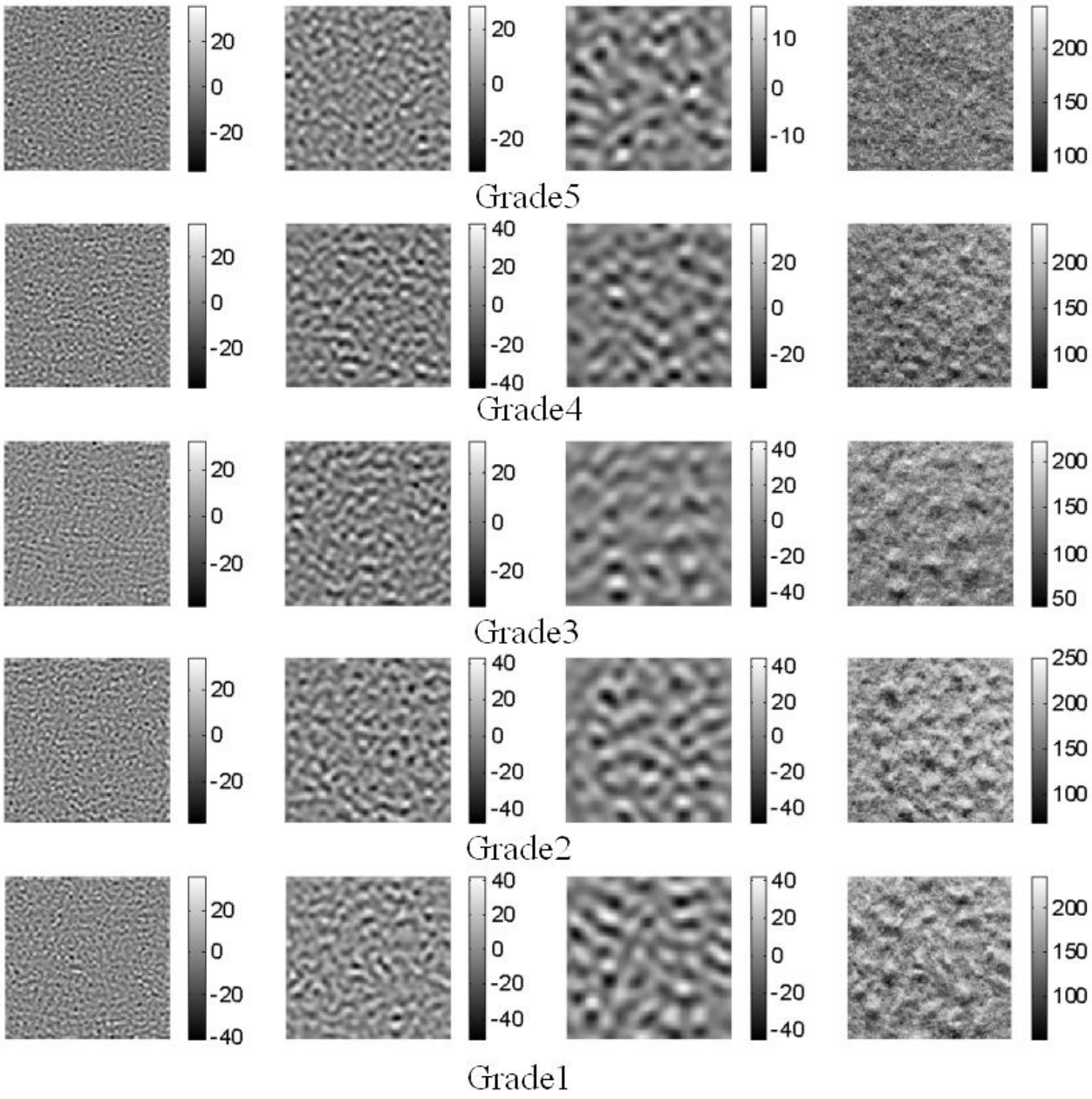

Figure 5. Reconstructed scale 4-6 detail images and original images of Grade 1-5 samples

Pilling evaluation using Multi-Layer Perception neural network

The MLP neural network is a data driven self-adaptive method that can adjust itself to the data without any explicit assumption about the data. It can also approximate any function with arbitrary

accuracy [8]. Since the pilling evaluation seeks a functional relationship between the pilling feature vector and the pilling grade, accurate identification of the underlying function by the MLP neural network will undoubtedly improve the prediction capacity of the pilling evaluation method.

According to the neural network literature [9], more than one hidden layer is rarely needed. The number of hidden neurons NH in the hidden layer is frequently stated to be dependent upon the number of input neurons NI and the number of output neurons NO of the network. The following equation has been suggested for determining the number of hidden neurons [9]:

$$NH = \frac{NI + NO}{2} \qquad (2)$$

Based on above analysis, an MLP neural network classifier with one input layer, one hidden layer and one output layer was designed as shown in Figure 6. The 18 pilling features are used as the input to the MLP.

The parameters for the MLP are:

Number of input features R=18; number of input neurons S^1=18;

Number of hidden neurons S^2=12; number of output neurons S^3=5;

Activation function is linear for input neurons (f^1), tan-sigmoidal for hidden neurons (f^2), and log-sigmoidal output neurons (f^3). The input to layer 2 is a^1; the output of layer 2 is a^2; the output of the third layer, a^3, is the network output of interest, and has been lapelled as y.

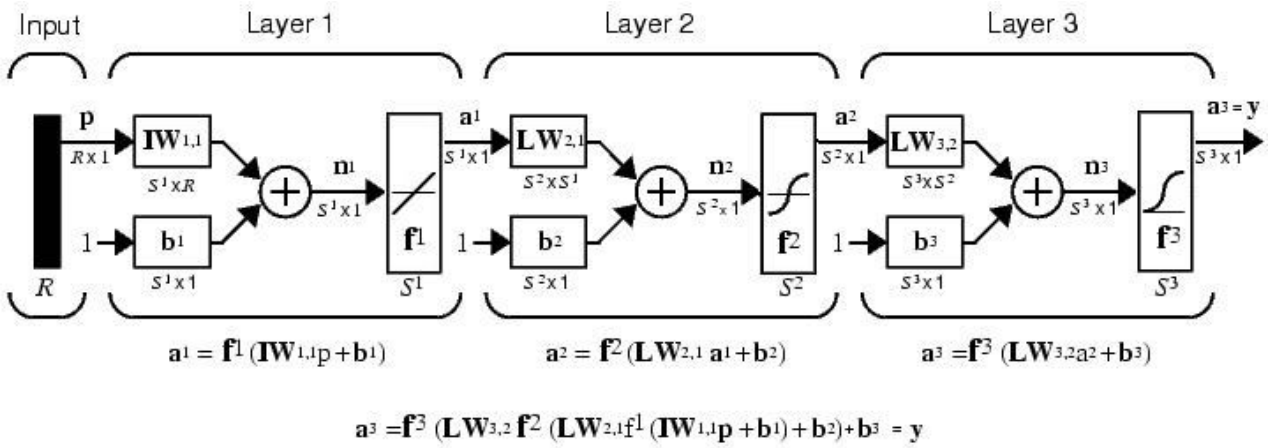

Figure 6. Representation of the MLP classifier [10]

The MLP is initialized by initialization function **initlay** [10]. The Levenberg-Marquardt back-propagation algorithm was used to train the network. The training function is **trainlm** [10]. The performance function is **mse** (mean squared error performance function.) [10]. The training results are stored in weight matrix $IW_{1,1}$, $LW_{2,1}$ and $LW_{3,2}$, and bias vector b^1,b^2,b^3.

The parameters for the training function are:

epochs: 100 goal: 0.0001 show: 25 time: Inf max_fail: 5 mem_reduc: 1

min_grad: 1.0000e-010 mu: 0.0010 mu_dec: 0.1000 mu_inc: 10 mu_max: 1.0000e+010

The training of the MLP neural network classifier is stopped as the training goal is reached. The training performance of the MLP is equal to 5.12e-005 after 25 iterations. Table 2 presents the MLP training outputs of the 20 samples. They have been successfully classified into 5 grades. The results are rounded to 3 decimal places.

Sample No	Output neurons				
	1	**2**	**3**	**4**	**5**
1	0.992	0.002	0.000	0.002	0.000
2	0.991	0.003	0.000	0.002	0.000
3	0.995	0.001	0.000	0.011	0.000
4	0.992	0.002	0.000	0.002	0.000
5	0.002	0.997	0.000	0.000	0.001
6	0.002	0.997	0.000	0.000	0.001
7	0.002	0.997	0.000	0.000	0.001
8	0.002	0.997	0.000	0.000	0.001
9	0.000	0.000	0.979	0.007	0.016
10	0.000	0.000	0.980	0.008	0.015
11	0.000	0.000	0.979	0.007	0.016
12	0.000	0.000	0.979	0.008	0.016
13	0.008	0.000	0.005	0.984	0.000
14	0.008	0.000	0.005	0.984	0.000
15	0.009	0.000	0.004	0.981	0.000
16	0.007	0.000	0.006	0.985	0.000
17	0.000	0.002	0.007	0.000	0.995
18	0.000	0.002	0.007	0.000	0.995
19	0.000	0.002	0.007	0.000	0.995
20	0.000	0.002	0.007	0.000	0.995

Table 2. MLP neural network classifier training outputs (samples No. 1-4: grade 1, No. 5-8: grade 2,etc.)

CONCLUSION

Based on the analysis of the Woolmark® SM 50 Blanket pilling test image set, the pilling was identified as being primarily present in the scale 4, 5 and 6 detail images. The scale 1, 2 and 3 detail images represented the image high frequency noise and random fiber structure, and hence, were excluded. The scale 7 detail and scale 7 approximation images represented the image low frequency fabric surface unevenness and background illumination variance, and hence, were also excluded. The principal component analysis of the pilling feature vectors extracted from the six direction detail sub-images at scales 4 to 6 shows that the pilling feature vectors, which measure the

pilling volume distribution at different directions and scales, have the ability to discriminate the different grades of pilling intensity. The neural network classification results further verify that ability of the pilling identification and characterization method.

The combination of the pilling identification, characterization method and neural network supervised classifier produces an objective method to evaluate the nonwoven fabric pilling intensity.

Acknowledgement

This work was carried out through a PhD scholarship awarded to the first author under the China Australia Wool Innovation Network (CAWIN) project. Funding for this project was provided by Australian wool producers and the Australian Government through Australian Wool Innovation Limited.

The standard pilling test images presented in this paper are the copyright property of The WoolMark Company and reproduced with their permission.

References

1. **"Annual Report-2003 Highlights-Textiles", Wool Research Organization of New Zealand, Christchurch, New Zealand, 2003.**

2. **M. Latifi, H. S. Kim, and B. Pourdeyhimi, *Textile Research Journal*, 71,7, 640 (2001).**

3. **S. Palmer and X. Wang, in "Computational Textile" (X. Zeng, Y. Li, D. Ruan, and L. Koehl, Eds.), pp. 23, Springer, Berlin, 2007.**

4. **I. W. Selesnick, R. G. Baraniuk, and N. G. Kingsbury, *IEEE Signal Processing Magazine*,11, 123 (2005).**

5. **S. Cai and K. Li, "Wavelet software", Polytechnic University, Brooklyn, NY, 2007.**

6. **"MATLAB", The MathWorks Inc., 2004.**

7. **"MATLAB Wavelet Toolbox", The MathWorks Inc., 2004.**

8. **K. Hornik, *Neural Networks*,4, 251 (1991).**

9. **"Best Practice Guidelines for Developing Neural Computing Applications", Electronics and Engineering Division, Department of Trade and Industry, London, UK, 2004.**

10. **"MATLAB Neural Network Toolbox", The MathWorks, Inc., 2004.**